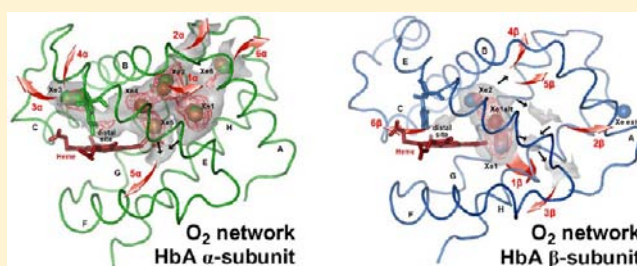# Effective Simulations of Gas Diffusion Through Kinetically Accessible Tunnels in Multisubunit Proteins: O$_2$ Pathways and Escape Routes in T-state Deoxyhemoglobin

Maria S. Shadrina, Ann M. English,* and Gilles H. Peslherbe*

Department of Chemistry and Biochemistry and Centre for Research in Molecular Modeling, Concordia University, 7141 Sherbrooke Street West, Montreal, Quebec, Canada H4B 1R6

Ⓢ Supporting Information

ABSTRACT: The diffusion of small gases to special binding sites within polypeptide matrices pivotally defines the biochemical specificity and reactivity of proteins. We investigate here explicit O$_2$ diffusion in adult human hemoglobin (HbA) as a case study employing the recently developed temperature-controlled locally enhanced sampling (TLES) method and vary the parameters to greatly increase the simulation efficiency. The method is carefully validated against standard molecular dynamics (MD) simulations and available experimental structural and kinetic data on ligand

diffusion in T-state deoxyHbA. The methodology provides a viable alternative approach to traditional MD simulations and/or potential of mean force calculations for: (i) characterizing kinetically accessible diffusion tunnels and escape routes for light ligands in porous proteins; (ii) very large systems when realistic simulations require the inclusion of multiple subunits of a protein; and (iii) proteins that access short-lived conformations relative to the simulation time. In the case of T-state deoxyHbA, we find distinct ligand diffusion tunnels consistent with the experimentally observed disparate Xe cavities in the α- and β-subunits. We identify two distal barriers including the distal histidine (E7) that control access to the heme. The multiple escape routes uncovered by our simulations call for a review of the current popular hypothesis on ligand escape from hemoglobin. Larger deviations from the crystal structure during simulated diffusion in isolated α- and β-subunits highlight the dampening effects of subunit interactions and the importance of including all subunits of multisubunit proteins to map realistic kinetically accessible diffusion tunnels and escape routes.

■ INTRODUCTION

The diffusion of small ligands within biological membranes and proteins is an essential process in living organisms. While small nonpolar molecules may freely permeate and diffuse within the lipid bilayers of cell membranes, diffusion within protein matrices likely occurs along well-defined hydrophobic tunnels.[1−4] Many proteins and enzymes reversibly bind or activate gases such as O$_2$, CO, NO, or H$_2$, and controlled access via the protein matrix of a specific gas to the active site is a critical component of a protein's function. Therefore, ligand diffusion pathways or tunnels, and the residues along such tunnels, can modulate protein activity by limiting the rate of ligand access to catalytic sites or other binding centers.

Gas diffusion is associated with transient thermal fluctuations of the polypeptide, and permanent tunnels are not observed in static protein structures.[3−5] However, molecular dynamics (MD) simulations provide detailed information on experimentally "invisible" gas trajectories. These have been characterized computationally using kinetic and thermodynamic approaches for numerous globins, including myoglobins (Mbs) from several species,[2,5−8] neuroglobin,[9] cytoglobin,[10] and monomeric hemoglobins.[2,11−14] The kinetic approach involves standard MD simulation of ligand diffusion, which

ideally requires a large number of independent replicate runs of ~100 ns so that statistical analysis of many independent trajectories yields a realistic description of ligand motion.[3] In the thermodynamic approach, the potential of mean force (PMF), or free energy landscape, is computed for a ligand at numerous points within the protein matrix.[3,11] Extensive sampling is essential to obtain accurate PMFs since incomplete analysis of rare or slow events, or the neglect of protein conformational changes, can result in large errors in the calculated barriers.[3,11] Therefore, while PMF calculations readily reveal inherent cavities that can stably accommodate ligands, they may fail to predict realistic ligand migration pathways between such cavities. Computational analysis of CO diffusion in myoglobin (Mb) serves as an illustration of how the kinetic[6] and thermodynamic approaches[7,8] can predict different ligand migration routes in proteins.

Tetrameric hemoglobin (Hb) plays a central role in mammalian physiology.[15] The Hb tetramer, which consists of two α- and two β-subunits, is a highly abundant red blood cell protein that transports O$_2$ from the lungs to the tissues. O$_2$
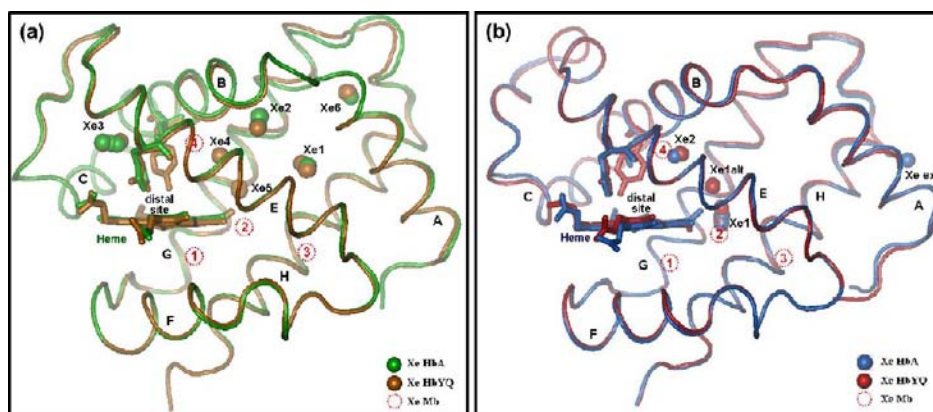
Figure 1. Experimental Xe docking sites found in the crystal structures of T-state deoxyHbA (PDB 2W6V) and T-state deoxyHbYQ (PDB 2W72).[16] (a) The α-subunit of HbA (green) superimposed on the α-subunit of HbYQ (orange). (b) The β-subunit of HbA (blue) superimposed on the β-subunit of HbYQ (red). HbA is adult human hemoglobin, and HbYQ is its LeuB10Tyr, HisE7Gln variant with mutations in both the α-subunit (L29Y, H58Q) and β-subunit (L28Y, H63Q). The experimental distances from the heme Fe (Å) and the fractional Xe occupancies (in parentheses) in the α-subunit are: αXe1, 14.2–14.3 (0.3–0.55); αXe2, 12.8–13.6 (0.35–0.6); αXe3, 8.7–9.4 (0.15–0.5); αXe4, 8.6 (0–0.2); αXe5, 8.6 (0–0.2); αXe6, 21.4 (0–0.9); and in the β-subunit: βXe1, 8.4 (0.9–1); βXe2, 9.8–9.9 (0.1–0.3).[16] The protein backbone atoms are shown in the ribbon representation, the Xe atoms are depicted as spheres, and the heme groups, as sticks. Additionally, the locations of the Xe atoms found in Mb crystals are shown as red dotted circles.

binds reversibly to a ferrous heme iron located ∼9 Å below the protein surface. Thus, the gas must diffuse within the globin matrix, and experimental Hb−ligand kinetics and equilibria cannot be fully interpreted without taking into account ligand diffusion pathways.[1]

O₂ diffusion in the isolated α-subunit of human Hb (HbA) was recently investigated by standard MD simulations,[17] but no studies on gas diffusion in the tetramer have been reported. Its 4-fold larger size relative to that of the monomeric globins would dramatically increase the computational time using current approaches. Also, complications arise because of spontaneous quaternary and tertiary transitions in the HbA tetramer at typical MD simulation times of ∼10−100 ns.[18] In preliminary studies, we found that the simulated HbA tetramer remained firmly representative of the quaternary and tertiary structure of T-state deoxyHbA during the first 2−3 ns of the MD simulations. Therefore, we sought methodology that would characterize gas diffusion pathways in the HbA tetramer within a few nanoseconds. We selected all-atom MD simulations that implement the temperature-controlled locally enhanced sampling (TLES) method,[19] since this allows an efficient study of ligand motion through a protein matrix by examining multiple noninteracting copies of the ligand in each simulation. Importantly, we observed that decreasing the Langevin damping coefficient, γ, accelerates ligand diffusion without altering the polypeptide backbone dynamics.

We now report the kinetically accessible O₂ diffusion tunnels in T-state deoxyHbA, an experimentally stable, but computationally unstable,[18] conformation of the HbA tetramer. We found that 2-ns simulations allowed the ligands to sample protein conformations within a purely T-state HbA ensemble and to fully define the O₂ diffusion tunnels, which are identical for TLES and normal ligands.

Crystallization of proteins under high pressures of Xe is frequently used to identify inherent ligand docking sites within their matrices. Xe cavities have been located experimentally and computationally in many monomeric globins,[2−13,20] and recently, the Xe docking sites shown in Figure 1 were identified in crystals of HbA and variant.[16] Therefore, we also investigated

Xe diffusion in T-state deoxyHbA to contrast the computed and experimental Xe docking sites.

■ METHODS

Simulation of Ligand Diffusion Using Temperature-Controlled Locally Enhanced Sampling (TLES). The locally enhanced sampling (LES) technique,[5] which is based on the time-dependent Hartree approximation,[21] was developed to study ligand diffusion in proteins.[3,13] Enhanced sampling is accomplished through the use of multiple copies of the ligand, which move independently of each other. The protein and water molecules, however, experience an average potential from all copies of the ligand. During simulations, ligands gain an average kinetic energy $\langle K_{LES} \rangle$ that depends on the temperature T and their copy number $N(\langle K_{LES} \rangle = 3/2Nk_BT)$.[22] Thus, 15 LES ligands (the N used here) travel at an effective temperature of 4500 K when T = 300 K.

To control their effective temperature, the LES ligands and the protein + water system are coupled to baths at different temperatures.[19,23] In the TLES approach,[19] the ligand and protein + water baths are set at T/N and T, respectively, but the hotter protein + water bath heats the ligand. The extent of heat transfer depends on the Langevin damping coefficient, γ. For example, with T/N = 21 K and γ = 5 ps^{-1}, we found that the effective temperature of TLES ligands is ∼400 K. At this temperature the ligands possess more realistic velocities, but it hinders their barrier crossing. On decreasing γ to 0.5 ps^{-1} (corresponding to an effective ligand temperature of ∼2000 K), the O₂ diffusion pathways are described within 2 ns, rendering longer simulation times unnecessary (see Method Validation).

The TLES algorithm as implemented in the NAMD 2.7 program[24] was employed here. The recent neutron-diffraction structure of T-state deoxyHbA 2DXM[25] was chosen as the initial structure for all-atom MD simulations performed at 310 K in explicit solvent. Details of the MD protocols, timings, simulation parameters, and ligand and HbA models are described in the Supporting Information (SI).

To thoroughly investigate the diffusion tunnels originating from the hemes, 15 TLES O₂ molecules were placed in sites close to the α1- (α-distal, αXe3, and αXe4 sites) and β1-hemes (β-distal and βXe2 sites), and a single normal O₂ molecule was similarly placed in each of the three remaining subunits of the HbA tetramer (Figures 1 and S1 [SI]). Fifteen TLES Xe atoms were placed at the same locations with the exception of the distal sites, which are not occupied by Xe in the HbA crystals.[16] The diffusion of 15 TLES O₂ molecules in isolated α- and β-subunits of deoxyHbA (monomeric models) was additionally simulated to establish the influence of subunit interactions on ligand
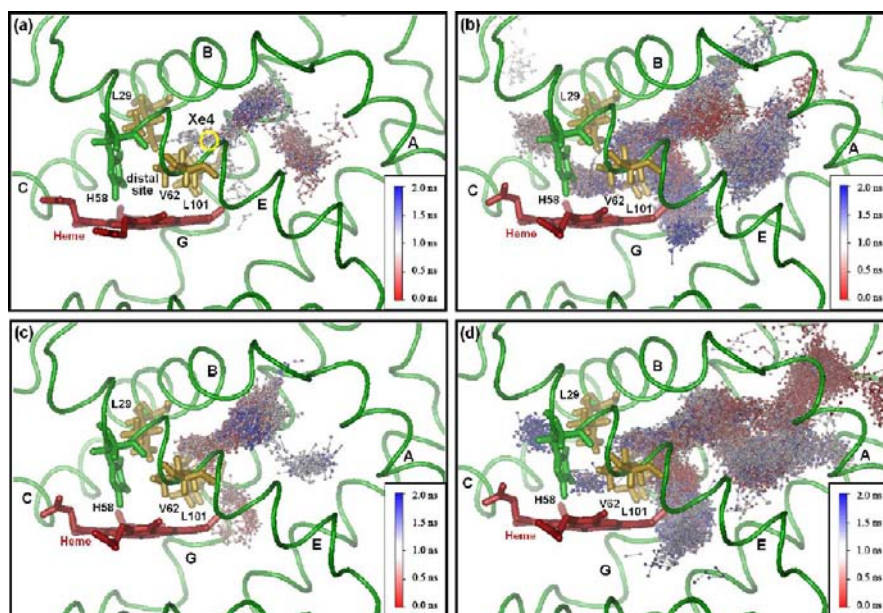
Figure 2. Method validation: comparison of time maps in the simulated diffusion over 2 ns of normal and TLES O_2 molecules in the α-subunit of T-state deoxyHbA and the isolated α-subunit. A single normal O_2 or 15 TLES O_2 molecules were initially placed in the αXe4 site (panel a, yellow circle). The heat maps indicate the positions (ball and stick) vs simulation time of (a) a normal O_2 molecule (standard MD simulation), $\gamma = 0.5$ ps^{-1}; (b) 15 TLES O_2 molecules, $\gamma = 0.5$ ps^{-1}; (c) 15 TLES O_2 molecules, $\gamma = 5$ ps^{-1}; (d) 15 TLES O_2 molecules in the isolated α-subunit, $\gamma = 0.5$ ps^{-1}. The backbone atoms of HbA are shown as a ribbon, the heme group as red sticks, the distal H58α (E7) as green sticks, and the ligand barrier B10E11G8 (residues L29α, V62α, L101α) as amber sticks. Ligand loading of the HbA subunits is shown in Figure S1 (SI).

diffusion. Table S3 (SI) summarizes the HbA models examined, the initial ligand positions, and the simulation parameters used.

Time and Density Maps of Ligand Diffusion. The simulation results are presented as time and density maps built by the VMD package.[26] Time maps plot ligand localization and exits from the protein vs simulation time. Density maps delineate the distribution of the simulated ligands on a grid of points spaced at 1 Å over the protein matrix. A more detailed discussion of the density maps is provided in the SI.

RESULTS

Method Validation. *Comparison of TLES and Standard MD Simulations.* Superimposition of 24 normal and 30 TLES O_2 trajectories (Figure S2 [SI]) reveals that they are very similar. Thus, the TLES algorithm maps the same kinetically accessible diffusion tunnels in the HbA tetramer as the standard MD simulations. Figure 3a compares the displacements during the simulations of the backbone carbon and nitrogen atoms of subunits containing normal or TLES O_2 molecules. The rmsd values are clearly insensitive to ligand loading, indicating that the TLES technique significantly improves sampling of HbA's diffusion tunnels (b vs a of Figure 2 and Figures S3b vs S3a [SI]) by decreasing the simulation time without influencing the backbone dynamics.

Lowering the Damping Coefficient, γ, from 5 to 0.5 ps^{-1}. TLES O_2 ligands with an effective temperature of 400 ($\gamma = 5$ ps^{-1}) exhibit similar trajectories as a normal O_2 ligand at 310 K (Figure 2a,c). Setting γ to 0.5 ps^{-1} raised the effective ligand temperature to ~2000 K, allowing the TLES O_2 to fully sample the α- (b vs c of Figure 2) and β-subunits (b vs c of Figure S3 [SI]) and several molecules escaped to the solvent during each 2-ns simulation. The rmsd values reveal that displacements of the backbone atoms of the tetramer were comparable with both γ values (Figure 3b). We emphasize that protein conformations were sampled within a temperature range of 309 ± 1 K. The

traveling ligands do not carve out new tunnels but rather promote the opening of tunnels between inherent cavities. Therefore, raising the effective temperature of the ligands increases their intercavity transition rates but does not alter the protein dynamics.[14,23] In sum, the TLES approach provides comparable results to standard MD simulations at a much reduced computational cost.

Computed vs Experimental Xe Cavities. The ability to realistically model Xe diffusion in HbA serves to further benchmark our methodology. Fifteen TLES Xe copies placed in the αXe4 and βXe2 sites visited all the experimental Xe cavities in 8 ns except αXe3 (Figures 1 and S8 [SI]). The latter is separated from αXe4 by the distal steric barriers discussed below. Thus, the kinetically accessible Xe sites of high density (Figure S8 [SI]) correspond to the thermodynamically favorable cavities that bind Xe atoms in crystals of T-state HbA and HbYQ (Figure 1). Small cavities were additionally visited in our simulations by the O_2 ligands (Figure 5). Such cavities observed computationally but not experimentally are referred to as phantom sites.[4,17] The O_2 ligands also sample the distal heme sites of both subunits (Figure 5).

Diffusion in the T-State deoxyHbA Tetramer. Protein–O_2 contacts maps, built assuming a collision occurred each time a protein atom and an O_2 ligand were within ≤2.5 Å (Figure S5 [SI]), reveal that the diffusion pathways in HbA are highly hydrophobic. Mainly Leu and Val residues line the tunnels as in the monomeric globins.[2] Using 15 TLES O_2 in each simulation, we found that the O_2 diffusion tunnels are fully defined after 1 ns, O_2 cavity occupancies are established between 1 and 2 ns, and several O_2 escape from HbA within 2 ns (Figure S7 [SI]). The convergence of ligand positions and densities in eight independent replicate simulations that map 120 TLES O_2 trajectories in each subunit is demonstrated in Figure S4 (SI). Since no ligands migrated between the α- and β-subunits, we now discuss diffusion in each subunit separately.
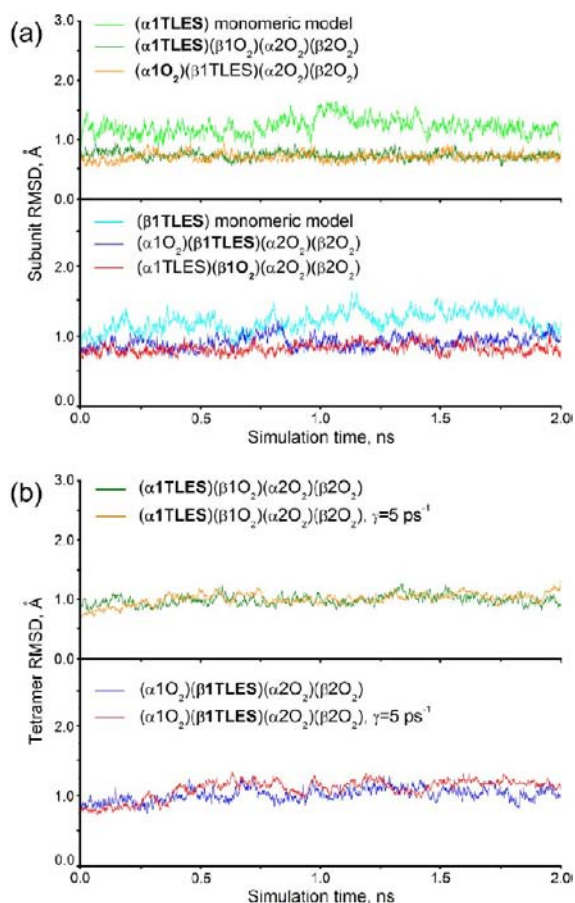
Figure 3. Method validation: root-mean-square deviations (rmsd, Å) of the backbone atoms during the MD simulations in Figures 2 and S3 (SI). The rmsd values at $t = 0$ ns are those of the equilibrated protein structures vs the crystal structure (PDB 2DXM).[25] (a) rmsd plots of the backbone atoms of the $\alpha 1$- (top panel) and $\beta 1$-subunits (bottom panel) of tetrameric (T-state deoxyHbA) and monomeric (isolated subunits) models. The $\alpha 1$- and $\beta 1$-subunits contain 15 TLES O_2 or single normal O_2 molecules. (b) rmsd plots of all backbone atoms in the T-state HbA tetramer containing 15 TLES O_2 molecules in the $\alpha 1$-subunit (top panel), the $\beta 1$-subunit (bottom panel) and one normal O_2 in the three remaining subunits (Figure S1 [SI]); $\gamma = 0.5$ or 5 ps^{-1} where indicated.

O_2 Diffusion from the $\alpha Xe4$, $\alpha Xe3$ and α-Distal Sites. Starting from the $\alpha Xe4$ site, the TLES O_2 molecule diffused over a long spiral-shaped tunnel (α-tunnel), thoroughly sampling the $\alpha Xe1$, $\alpha Xe2$, $\alpha Xe4$, and $\alpha Xe5$ sites (Figure 4a). Distal barriers (E7 and B10E11G8), which control ligand diffusion to and from the α-distal site, are defined by regions of low ligand occupancy (Figure 5a). Due to the presence of these barriers, the α-distal heme pocket was better sampled from its constitutive $\alpha Xe3$ and α-distal sites (Figure 4b,c). Regions of highest O_2 density overlap the experimental Xe cavities, which can be considered as O_2 binding sites (Figures S4a, S7a [SI]). Diffusion is essentially barrierless in the α-tunnel given the high O_2 density between docking sites (Figure 5a), whereas the E7 barrier clearly divides the α-distal heme pocket into the $\alpha Xe3$ and α-distal sites. An additional barrier, G16H8A11, separates the α-tunnel and the $\alpha Xe6$ cavity as indicated by the low O_2 sampling of this boundary (Figure 4a−c). In contrast, heavier Xe ligands sample the $\alpha Xe6$ cavity extensively (Figure S8a [SI]).

During eight simulations (Figure S4a [SI]) 47 of 120 TLES O_2 molecules escaped to the solvent. Figure 5a shows the six α-portals used by these ligands, and the residues and helices defining the portals are listed in Table S4 (SI). Since the ligands diffuse extensively within the protein matrix before escaping, their starting positions do not alter the tunnel network or dictate their exit portal. For example, O_2 molecules placed in either $\alpha Xe4$ or $\alpha Xe3$ (Figure 4a,b) escaped via portal 2α.

O_2 Diffusion from the $\beta Xe2$ and β-Distal Sites. The time maps (Figure 4d,e) show that from these sites most of the ligands diffuse into a short tunnel encompassing the experimental $\beta Xe1$, $\beta Xe1alt$, and $\beta Xe2$ sites (β-tunnel). The β-tunnel is the region of highest O_2 density within the β-subunit and possesses a number of poorly accessible satellite cavities (Figure 5b). O_2 diffusion from the β-distal site to the β-tunnel or directly to the bulk solvent is controlled by barriers B10E11G8 and E7, respectively. In the absence of a β-analogue of $\alpha Xe3$, the β-distal heme pocket corresponds to the β-distal site and has dramatically lower O_2 occupancy than the α-pocket (Figure 5).

Of the 120 TLES O_2 trajectories mapped in Figure S4b (SI), 88 molecules escaped from the β-tunnel through portal 1β to the large water-filled central cavity of HbA (Figure 5b, Table S4 [SI]). Most of these ligands re-entered the same β-subunit one or more times before escaping to the bulk solvent, and a few also entered the opposite β-subunit. Five minor β-portals were observed, and all lead directly to the bulk solvent. Only 1−2 TLES O_2 molecules escaped through each of the minor portals (Figure 5b, Table S4 [SI]), including portal 6β, which is the shortest path to the solvent from the β-pocket.

O_2 Diffusion in the Isolated α- and β-Subunits. The elimination of neighboring subunits removes functional and structural H-bonds at the interfaces.[27] Thus, as expected, the isolated deoxyHbA subunits exhibited rmsd values ∼0.1−1 Å greater than those of the tetramer over 2-ns simulations (Figures 3a). Notably, the isolated α-subunit starting from the R-state coordinates is reported to be conformationally stable,[17] but the published rmsd values are not referenced to the crystal structure, preventing comparison with the present results.

The O_2 tunnel networks are similar overall in the tetramer and monomers. Enhanced conformational flexibility increases O_2 migration as reflected in the wider α-tunnel and high occupancy of $\alpha Xe6$ in the isolated vs bound α-subunit (d vs b of Figure 2). Most O_2 molecules escape from the isolated α-subunit via portal 6α (Table S4 [SI]), and in the isolated β-monomer (Figure S3d [SI]) a new minor portal (m) opened up that is blocked by the neighboring α-subunit in tetrameric HbA (Table S4 [SI]). Since it is impossible to predict *a priori* the effects of subunit interactions, realistic simulations of ligand diffusion demand use of a protein's native oligomeric structure, which is facilitated by the approach described in this work.

◼ DISCUSSION

Kinetically Accessible Gas Diffusion Tunnels: Characterization and Validation. Combining the TLES method with Langevin dynamics and a damping coefficient γ of 0.5 ps^{-1} allowed the efficient study of gas diffusion within a large protein matrix via a series of short simulations. Different initial velocities and independent ligand trajectories, as well as varied Langevin random forces in the replicates, enhanced sampling of the diffusion tunnels in T-state deoxyHbA. Specifically, monitoring of O_2 migration and escape and the temporal evolution of maximum density revealed that the O_2 diffusion
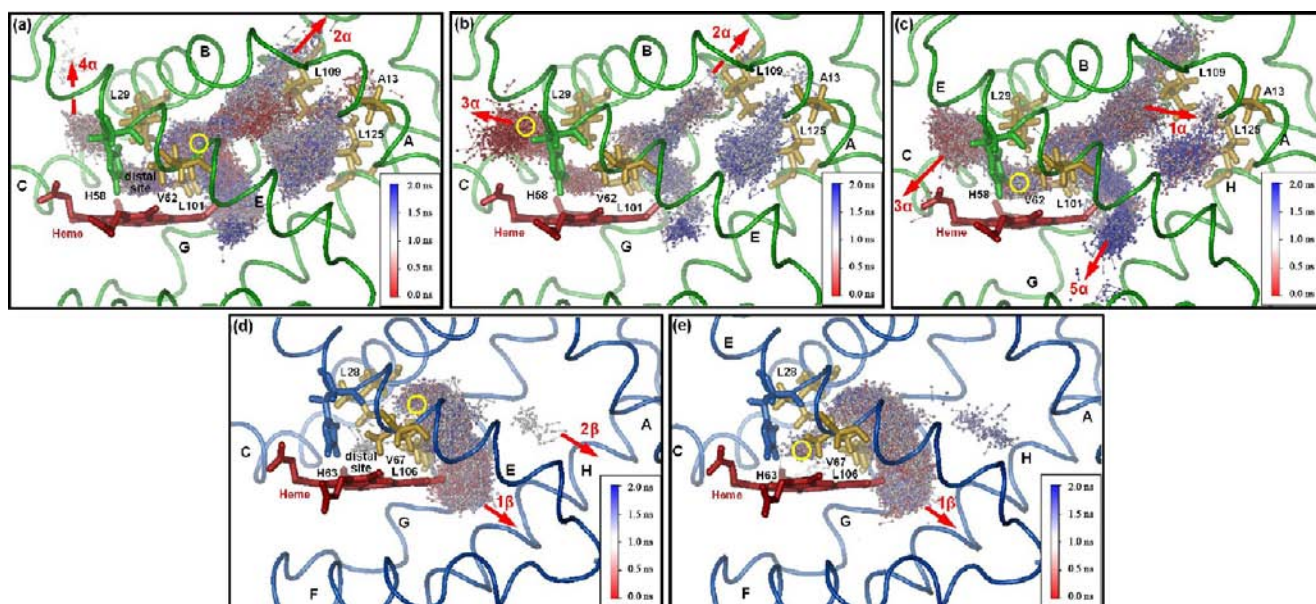
Figure 4. Time maps for 2-ns MD simulations of the diffusion of 15 TLES O_2 molecules in T-state deoxyHbA. Trajectories from the (a) αXe4, (b) αXe3 and (c) α-distal sites in the α-subunit, and (d) βXe2 and (e) β-distal sites in the β-subunit. The yellow circle in each panel indicates the initial positions of the TLES O_2 molecules. The heat maps indicate O_2 position vs simulation time. The red arrows locate O_2 exit portals from the polypeptide (Figure 5, Table S4 [SI]). The backbone atoms of HbA are shown as green (α-subunit) or blue (β-subunit) ribbon, the heme as red sticks, and the distal barriers E7 as green (H58α) or blue (H63β) sticks and B10E11G8 as amber sticks. An additional ligand barrier separating the αXe1 and αXe6 cavities (see text), G16H8A11 (residues L109α, L125α, A13α), is shown as amber sticks.
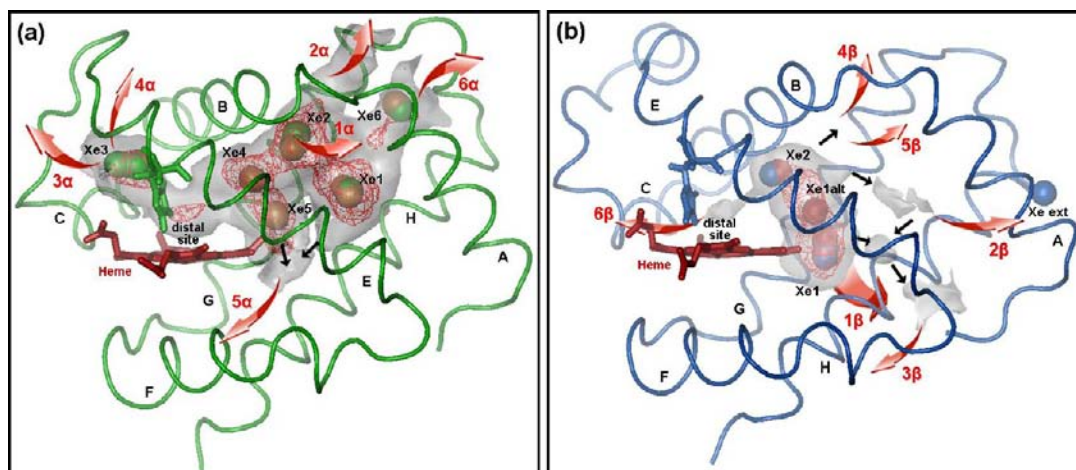

Figure 5. Kinetically accessible O_2 diffusion tunnels (gray isospheres), regions of high O_2 maximum density (red isosurfaces), and exit portals (red arrows) found in eight replicate 2-ns simulations of the diffusion of 15 TLES O_2 molecules in the (a) α-subunit and (b) β-subunit of T-state deoxyHbA. The high O_2 density regions overlap the experimental Xe docking sites (solid spheres as in Figure 1). Black arrows indicate the paths of O_2 diffusion between the cavities. From 120 trajectories per subunit (Figure S4 [SI]), the numbers of O_2 molecules that escaped via each portal are as follows: 1α (7), 2α (11), 3α (18), 4α (3), 5α (3), 6α (5), 1β (88), 2β (1), 3β (1), 4β (1), 5β (2), 6β (2). Note that 73% of the O_2 molecules exit via portal 6α in the isolated α-subunit (Table S4 [SI]). Portals lead directly to the bulk solvent except dominant portal 1β, which conducts O_2 to the central water-filled cavity of HbA. The protein representation is described in the caption of Figure 4.

tunnels can be mapped in 2 ns (e.g., Figure S7 [SI]). Our multiple simulations with varied initial O_2 positions (i.e., five docking sites close to the hemes) ensured that the ligands sampled tunnel regions separated by steric barriers and discovered several escape routes from the protein (Figure 5, Table S4 [SI]).

The convergence of eight replicate simulations per subunit (Figure S4 [SI]) suggests that we have reliably charted kinetically accessible O_2 diffusion tunnels in the T-state deoxyHbA tetramer. Next, we question if there is experimental evidence to support these networks shown in Figure 5. To

locate internal hydrophobic cavities, Savino et al. soaked crystals of T-state deoxyHbA under 10 atm Xe and observed several Xe docking sites within its polypeptide (Figure 1).[16] Our methodology correctly predicts all of the experimental Xe docking sites (Figures 5 and S4 [SI] vs Figure 1), and as proposed by Savino et al., these sites define ligand migration pathways between the heme and solvent (Figure 5). It has long been proposed that the Xe cavities observed in Mb link with transient fluctuations of the polypeptide to form ligand diffusion pathways, and an abundance of experimental evidence supports this view (reviewed in ref 4).

Ligand Barriers and Portals. Widespread among the globins, distal barriers corresponding to E7 and B10E11G8 control access to the distal heme pocket.[28−30] Marked by regions of low ligand occupancy or density (Figures 5, S4 [SI]), these distal barriers, combined with steric hindrance in the distal site, appear to discriminate against the large-diameter Xe atoms (see Diffusion of Mass-Exchanged ^{32}Xe and ^{131}O$_2$ in the SI).

E7 forms a visible ligand barrier in the static crystal structures of Hb and Mb. This led Perutz and Mathews to hypothesize over 45 years ago that swinging of E7 between closed and open conformations controls O$_2$ exchange between the heme and solvent.[31] Ligands purportedly escape only when the E7 channel (delineated by the pathways that traverse the E7 barrier) is open.[29,31,32] The E7 channel is closed in both subunits in the crystal structure of T-state deoxyHbA (2DXM)[25] and did not spontaneously open during any of our simulations. Cohen and Schulten reported that the E7 channel also remained closed in their 10−25 ns simulations of O$_2$ diffusion in Mb and concluded that swinging of the E7 gate is unlikely a critical factor in the regulation of O$_2$ exit or entry to Mb.[2] In support of this view, we observed that 23 O$_2$ molecules escaped through the *closed* E7 channels (portals 3α, 4α, and 6β; Figure 5 and Table S4 [SI]).

Barrier B10E11G8 controls O$_2$ diffusion between the distal site and the interior α- and β-tunnels (Figure 4). These tunnels possess several escape portals, but the truncated β-tunnel appears optimized for efficient ligand transport between the β-distal site and HbA's central cavity. Remarkably, 73% of the O$_2$ molecules placed in the β-subunit entered the central cavity via portal 1β (Figure 5, Table S4 [SI]) and returned to the β-tunnel or escaped to the bulk solvent. In contrast, only 2% escaped via the closed β-E7 channel. Barrier G16H8A11 gates access to the αXe6 cavity and portal 6α, the major exit point found experimentally and computationally[17] (Figure 2d, Table S4 [SI]) from the isolated α-subunit.

Importantly, no O$_2$ or Xe ligands crossed the α,β-subunit interfaces. This leads us to speculate that kinetically accessible *intersubunit* diffusion tunnels extending from the hemes would trap O$_2$ for excessive periods and possibly decouple its release from metabolic demand.

We emphasize that the portals in our model connect regions of high O$_2$ occupancy to the solvent (or HbA's central cavity in the case of portal 1β). In other words, portals adjacent to high-density sites are the most probable escape routes from T-state deoxyHbA (Figure 5 and Table S4 [SI]). Thus, more molecules escaped from the protein via the highly occupied α- and β-tunnels than via the E7 channels (Figure 5 and Table S4 [SI]). Statistical analysis of hundreds of replicate simulations (which is outside the scope of this work) would more rigorously determine the probability of escape via each portal. However, we predict that the same preferred exit portals (1β, 1α−3α; Figure 5, Table S4 [SI]) would emerge from a full analysis because these are determined by the statistical ligand distribution.

Our results are clearly at odds with the still popular hypothesis of Perutz and Mathews[31] that ligands escape from Hb and Mb mainly via open E7 channels. This hypothesis, based on static structures, is less compelling in light of the diffusion tunnels reported here and for other globins.[2,4−14] Controlled by protein dynamics, individual ligands diffuse randomly and independently between inherent docking sites, leading to significant fluctuations in both escape times and

routes. However, ligand distribution over the protein matrix is statistically stationary when we consider many ligand trajectories. Thus, the exit portal from a given initial position is not predetermined as exemplified by the escape via the α-tunnel as well as the E7 channel of O$_2$ molecules placed in αXe3 (Figure 4b). Importantly, mutation of residues in HbA may lead to altered ligand distributions as revealed in our preliminary analysis of TrpE7 mutants (data not shown). Access to both the E7 channel and interior channels can be blocked in these mutants, depending on the conformation of the indole side chain. Thus, an examination of both simulated diffusion and static mutant structures should provide a more complete interpretation of published kinetic data on ligand association with HbA variants.[32−34]

Migration of Photodissociated Ligands in T-state DeoxyHbA. Photolysis of heme-bound ligands has been used extensively to experimentally map ligand diffusion pathways. The photodissociated ligand is free to migrate within the protein, and its location can be directly monitored by X-ray analysis. Photolysis studies starting from heme-ligated Hb generally report on the R-state since ligand migration is rapid relative to the R to T transition. However, substitution of Ni^{II} for Fe^{II} in either the α- or β-hemes locks the hybrid Hb tetramer in the T-conformation.[35,36] Furthermore, ligand migration can be selectively examined in each subunit since the Ni porphyrins do not bind O$_2$, CO, or NO and no metal exchange was observed.[35,36]

A cryogenic structural study showed that under continuous photolysis of the Fe−CO bond, CO migrated to the βXe2 site of Hb[α(Ni)β(Fe-CO)]$_2$ but remained in the α-distal site of Hb[α(Fe-CO)β(Ni)]$_2$,[37] consistent with the relative computed O$_2$ occupancies of the α- vs β-distal site (Figures 4 and 5). Realistic migration times obtained from our standard MD simulations indicate that 10 normal O$_2$ molecules placed in the β-distal site migrated to the β-tunnel in less than 0.5 ns. In contrast, six molecules diffused in 0.6−2 ns to the α-tunnel and αXe3 cavity while four still remained in the α-distal site after 2 ns. Thus, photodissociated CO is observed only in the T-state α-distal sites because, like O$_2$, it leaves these sites relatively slowly. The extent of ligand migration also determines the rates of geminate recombination with the heme. Notably, O$_2$ geminate recombination is considerably slower in the β- vs α-subunit,[38] again consistent with the rapid O$_2$ escape from the T-state β-distal site predicted by our simulations.

Studies by Olson and co-workers revealed that the kinetics of ligand binding to R-state HbA are not affected by high Xe pressure.[34] This led them to conclude that photodissociated ligands do not diffuse to Xe binding sites but remain in the distal heme pockets before escaping via the E7 channels. Since we observed rapid O$_2$ escape to interior tunnels, especially from the β-distal site, we examined diffusion in T-state deoxyHbA in the presence of Xe. A single Xe atom placed in αXe2 and βXe1, sites of highest Xe occupancy (Figure 1), had little effect on O$_2$ diffusion in either subunit (see discussion of Figure S6 [SI]). This is not surprising since the α- and β-tunnels in the HbA crystals each contain ∼1 Xe atom[16] that can diffuse between multiple locations (Figure 1).

Why Do the α- and β-Subunits Possess Dissimilar Kinetically Accessible Diffusion Tunnels? Functional differences between the α- and β-subunits, which possess highly conserved tertiary structures, have long been of interest.[39] An obvious question triggered by examination of Figure 5 is why the β-network is dramatically truncated

compared to the extensive α-network? Assuming, as proposed by Savino et al., that the Xe docking sites define ligand migration pathways between the heme and solvent,[16] a truncated β-tunnel could be predicted from the absence of experimental β-sites equivalent to αXe1, αXe2, and αXe6 (Figure 1). Structurally, diffusion between βXe2 and a site corresponding to αXe2 is blocked in the β-subunit by the αA63→βL68 and αY24→βV23 substitutions, and by βL110, which adopts a different conformation from that of αL105. Furthermore, the space filling substitutions, αA13→βL14 and αL125→βY130, plug the β-cavities analogous to αXe1, αXe2, and αXe6. Thus, rapid O_2 migration from the β-distal site to the β-tunnel combined with these substitutions suggest an evolutionary drive to expel O_2 from the T-state β-subunit into HbA's central cavity. One can speculate that in the crowded environment of the red blood cell, T-state HbA molecules align to channel O_2 through their central cavities to the outside of the cell. Alternatively, O_2 escape to tissues may be optimal via the central cavity when T-state HbA binds to the cell membrane. In support of this latter hypothesis, T-state HbA exhibits high membrane affinity.[40] In contrast, there is no portal to the central cavity in the T-state α-subunit, but O_2 can escape to the bulk solvent via several routes with similar probability (Figure 5 and Table S4 [SI]).

The mechanisms that decrease ligand affinity in T-state HbA appear to be designed to promote the escape patterns just described. Tension in the F-helix and other proximal constraints lower the ligand affinity of the T-state α-heme whereas steric hindrance by the distal residues (E7, E11) promotes ligand expulsion from the T-state β-distal site.[37] Nonheme bound ligands are better accommodated in the α-distal site as seen in Figure 5 as well as the reported higher fractional occupancy of water in this site.[41] O_2 molecules enter the E7 channel and the α-tunnel from the α-distal site with almost equal probability, which promotes escape via all the α-portals. Although intriguing, the physiological reasons for funneling O_2 escape mainly through one exit in the β-subunit vs several exits in the α-subunit of the T-state deoxyHbA tetramer are not obvious at present.

Ligand Diffusion in HbA vs Mb. Two (Xe2 and Xe4) of the four experimental Xe sites found in Mb[20] are in similar positions to HbA's βXe1 and βXe2 cavities (Figure 1). Xe1 and Xe3 do not correspond to any sites in HbA. In fact, Xe1 is part of Mb's proximal heme pocket,[20] but HbA possesses no proximal cavities.

A major diffusion tunnel in Mb,[6] encompassing the Xe4, Xe2, and Xe1 sites, connects via two narrow passages to a minor interior tunnel that contains Xe3 and a few phantom sites.[4] These tunnels span both the distal and proximal regions of Mb,[2,6–8] whereas the tunnels are concentrated in the distal halves of HbA's subunits (Figure 5). Notably, the distal portion of Mb's major tunnel encompassing the Xe4–Xe2 sites resembles both the β-tunnel and the segment of the α-tunnel containing the αXe4 and αXe5 sites.

At least nine portals were observed in Mb,[6–8] including portals 7 and 8[6] that correspond respectively to portals 2α,1α and 4β,5β in Figure 5. Three or more Mb portals may be under the control of the E7 barrier (distal H64), which guides ligands directly to the solvent. Mb's B10E11G8 barrier (residues L29, V68, I107) steers ligands from the distal site to the major tunnel.[4,6–8,29] Water but not Xe was found in Mb's distal heme site, indicating ligand discrimination similar to that found in T-state HbA.

CONCLUSIONS

Our TLES and standard MD simulations provide a realistic description of the kinetically accessible diffusion tunnels in T-state deoxyHbA that are consistent with the protein's experimentally observed Xe and photodissociated-CO docking sites. Pathways in the α-subunit guide ligands to the bulk solvent via multiple portals, but most O_2 molecules placed in the β-subunit are directed toward HbA's central cavity via a single portal. The simulated escape routes are consistent with the ligand distribution within the subunits but at odds with a popular hypothesis that swinging of E7 between closed and open conformations controls O_2 escape to the solvent. In contrast to the isolated subunits of many of the monomeric globins,[2] the proximal halves of HbA's subunits possess low O_2 porosity.

Overall, our intriguing findings suggest novel structure–function relationships in HbA that should stimulate further computational and experimental investigations. Importantly, we contend that the converged average densities reflect the statistical stationarity of O_2 distribution within the HbA tetramer, which dictates the escape routes. Finally, the methodology we have applied here to HbA could be used to efficiently study kinetically accessible gas diffusion tunnels in any multisubunit protein or multienzyme complex.

ASSOCIATED CONTENT

$\mathcal{S}$ Supporting Information

Simulation and validation details, table of observed O_2 exit portals, diffusion of mass-exchanged ^{32}Xe and $^{131}O_2$, O_2 diffusion in the presence of Xe, evolution of time and density maps of O_2 and Xe diffusion. This material is available free of charge via the Internet at http://pubs.acs.org.

AUTHOR INFORMATION

Corresponding Author
gilles.peslherbe@concordia.ca (G.H.P.); english@alcor.concordia.ca (A.M.E.)

Notes

The authors declare no competing financial interest.

ACKNOWLEDGMENTS

REFERENCES

(1) Berg, O. G.; von Hippel, P. H. *Annu. Rev. Biophys. Biophys. Chem.* **1985**, *14*, 131−160.
(2) Cohen, J.; Schulten, K. *Biophys. J.* **2007**, *93*, 3591−3600.
(3) Elber, R. *Curr. Opin. Struct. Biol.* **2010**, *20*, 162−167.
(4) Tomita, A.; Kreutzer, U.; Adachi, S.; Koshihara, S. Y.; Jue, T. *J. Exp. Biol.* **2010**, *213*, 2748−2754.
(5) Elber, R.; Karplus, M. *J. Am. Chem. Soc.* **1990**, *112*, 9161−9175.
(6) Ruscio, J. Z.; Kumar, D.; Shukla, M.; Prisant, M. G.; Murali, T. M.; Onufriev, A. V. *Proc. Natl. Acad. Sci. U.S.A.* **2008**, *105*, 9204−9209.
(7) Cohen, J.; Arkhipov, A.; Braun, R.; Schulten, K. *Biophys. J.* **2006**, *91*, 1844−1857.

(8) Maragliano, L.; Cottone, G.; Ciccotti, G.; Vanden-Eijnden, E. *J. Am. Chem. Soc.* **2010**, *132*, 1010−1017.

(9) Bocahut, A.; Bernad, S.; Sebban, P.; Sacquin-Mora, S. *J. Phys. Chem. B* **2009**, *113*, 16257−16267.

(10) Orlowski, S.; Nowak, W. *J. Mol. Model.* **2007**, *13*, 715−723.

(11) Cohen, J.; Olsen, K. W.; Schulten, K. *Methods Enzymol.* **2008**, *437*, 439−57.

(12) Daigle, R.; Rousseau, J. A.; Guertin, M.; Lague, P. *Biophys. J.* **2009**, *97*, 2967−2977.

(13) Golden, S. D.; Olsen, K. W. *Methods Enzymol.* **2008**, *437*, 459−475.

(14) Czerminski, R.; Elber, R. *Proteins: Struct., Funct., Bioinf.* **1991**, *10*, 70−80.

(15) Schechter, A. N. *Blood* **2008**, *112*, 3927−3938.

(16) Savino, C.; Miele, A. E.; Draghi, F.; Johnson, K. A.; Sciara, G.; Brunori, M.; Vallone, B. *Biopolymers* **2009**, *91*, 1097−1107.

(17) Lepeshkevich, S. V.; Biziuk, S. A.; Lemeza, A. M.; Dzhagarov, B. M. *Biochim. Biophys. Acta* **2011**, *1814*, 1279−1288.

(18) Hub, J. S.; Kubitzki, M. B.; de Groot, B. L. *PLoS Comput. Biol.* **2010**, *6*, e1000774.

(19) Cohen, J.; Kim, K.; King, P.; Seibert, M.; Schulten, K. *Structure (Cambridge)* **2005**, *13*, 1321−1329.

(20) Tilton, R. F., Jr.; Kuntz, I. D., Jr.; Petsko, G. A. *Biochemistry* **1984**, *23*, 2849−2857.

(21) Gerber, R.; Buch, V.; Ratner, M. *J. Chem. Phys.* **1982**, *94*, 3022−3030.

(22) Straub, J.; Karplus, M. *J. Chem. Phys.* **1991**, *94*, 6737−6739.

(23) Das, B.; Helms, V.; Lounnas, V.; Wade, R. C. *J. Inorg. Biochem.* **2000**, *81*, 121−131.

(24) Phillips, J. C.; Braun, R.; Wang, W.; Gumbart, J.; Tajkhorshid, E.; Villa, E.; Chipot, C.; Skeel, R. D.; Kale, L.; Schulten, K. *J. Comput. Chem.* **2005**, *26*, 1781−1802.

(25) Chatake, T.; Shibayama, N.; Park, S. Y.; Kurihara, K.; Tamada, T.; Tanaka, I.; Niimura, N.; Kuroki, R.; Morimoto, Y. *J. Am. Chem. Soc.* **2007**, *129*, 14840−14841.

(26) Humphrey, W.; Dalke, A.; Schulten, K. *J. Mol. Graphics* **1996**, *14*, 27−28.

(27) Lukin, J. A.; Ho, C. *Chem. Rev.* **2004**, *104*, 1219−1230.

(28) Samuni, U.; Dantsker, D.; Ray, A.; Wittenberg, J. B.; Wittenberg, B. A.; Dewilde, S.; Moens, L.; Ouellet, Y.; Guertin, M.; Friedman, J. M. *J. Biol. Chem.* **2003**, *278*, 27241−27250.

(29) Scott, E. E.; Gibson, Q. H.; Olson, J. S. *J. Biol. Chem.* **2001**, *276*, 5177−5188.

(30) Pesce, A.; Nardini, M.; Dewilde, S.; Geuens, E.; Yamauchi, K.; Ascenzi, P.; Riggs, A. F.; Moens, L.; Bolognesi, M. *Structure (Cambridge)* **2002**, *10*, 725−735.

(31) Perutz, M. F.; Mathews, F. S. *J. Mol. Biol.* **1966**, *21*, 199−202.

(32) Birukou, I.; Schweers, R. L.; Olson, J. S. *J. Biol. Chem.* **2010**, *285*, 8840−8854.

(33) Birukou, I.; Soman, J.; Olson, J. S. *J. Biol. Chem.* **2011**, *286*, 10515−10529.

(34) Birukou, I.; Maillett, D. H.; Birukova, A.; Olson, J. S. *Biochemistry* **2011**, *50*, 7361−7374.

(35) Luisi, B.; Shibayama, N. *J. Mol. Biol.* **1989**, *206*, 723−736.

(36) Luisi, B.; Liddington, B.; Fermi, G.; Shibayama, N. *J. Mol. Biol.* **1990**, *214*, 7−14.

(37) Adachi, S.; Park, S. Y.; Tame, J. R.; Shiro, Y.; Shibayama, N. *Proc. Natl. Acad. Sci. U.S.A* **2003**, *100*, 7039−7044.

(38) Shibayama, N.; Yonetani, T.; Regan, R. M.; Gibson, Q. H. *Biochemistry* **1995**, *34*, 14658−14667.

(39) Ho, C. *Adv. Protein Chem.* **1992**, *43*, 153−312.

(40) Walder, J. A.; Chatterjee, R.; Steck, T. L.; Low, P. S.; Musso, G. F.; Kaiser, E. T.; Rogers, P. H.; Arnone, A. *J. Biol. Chem.* **1984**, *259*, 10238−10246.

(41) Esquerra, R. M.; Lopez-Pena, I.; Tipgunlakant, P.; Birukou, I.; Nguyen, R. L.; Soman, J.; Olson, J. S.; Kliger, D. S.; Goldbeck, R. A. *Phys. Chem. Chem. Phys.* **2010**, *12*, 10270−10278.